Global. Each experiment has at least five global "parameters": (1) number of pulses/time point, (2) recycle time, (3) method to achieve steady state, (4) solvent suppression, and (5) receiver gain.

IV. Future Prospects

The ultimate goal of NMR investigations of biomolecules is to obtain structural and dynamic information. To this end, many specialized experimental techniques similar to those described above have been developed which allow the measurement of parameters that provide distance and dihedral angle constraints.[93,94] In conjunction with the methods described in this chapter, computer-automated resonance assignments and spectral analysis techniques should facilitate efficient studies of larger biomolecules and are expected to accelerate the pace of NMR contributions to structural biochemistry.

Acknowledgments

We thank Charles G. Hoogstraten for reviewing the manuscript. This work was supported by National Institutes of Health Grants RR02301 and GM35976. A.S.E. was supported by an NIH Biophysics Training Grant.

[93] G. Wagner, S. G. Hyberts, and T. F. Havel, *Annu. Rev. Biophys. Biomol. Struct.* **21,** 167 (1992).
[94] A. Bax and S. Grzesiek, *Acc. Chem. Res.* **26,** 131 (1993).

[2] Measurement of Homo- and Heteronuclear J Couplings from Quantitative J Correlation

By AD BAX, GEERTEN W. VUISTER, STEPHAN GRZESIEK, FRANK DELAGLIO, ANDY C. WANG, ROLF TSCHUDIN, and GUANG ZHU

Introduction

The utility of three-bond J couplings for determining backbone and side-chain conformation in peptides and proteins has long been established.[1] Historically, the focus has been primarily on three-bond ^1H–^1H couplings to obtain information on the dihedral backbone angle ϕ and on the side-chain torsion angle χ_1. The surge in the use of uniform ^{13}C and

[1] V. F. Bystrov, *Prog. NMR Spectrosc.* **10,** 41 (1976).

^{15}N enrichment for protein structural studies now also makes it possible to measure many of the heteronuclear J couplings. There are essentially three different approaches to the measurement of these small and frequently unresolved J couplings. The two established approaches, direct measurement and ECOSY-based measurement, are briefly discussed below. This chapter focuses, however, on a third method, referred to as quantitative J correlation. In this approach the J coupling is obtained from the fraction of magnetization that is transferred from a nucleus to its J-coupled partner.

In the direct measurement approach the J value is measured directly from the in-phase or antiphase splitting of a particular resonance in the one-dimensional (1D) or two-dimensional nuclear magnetic resonance (2D NMR) spectrum. In cases where J is smaller than the natural line width, this typically requires strong resolution enhancement and/or iterative fitting programs to obtain accurate J values.[2-4] Methods that fit the amplitude of a multiplet as a function of a dephasing time[5] and methods that use deconvolution of a multiplet with a reference multiplet[6] also fall in this category.

A second powerful approach to the measurement of unresolved J couplings is based on the so-called ECOSY principle.[7] Here, the unresolved J coupling between two nuclei A and B is measured from the relative displacement of the two resolved components of an AC cross-peak, which are displaced in one dimension of the n-dimensional (nD) spectrum by J_{AB} and in the other dimension by J_{BC}. Measurement of J_{AB} by this method requires the presence of a third spin, C, which must have a well-resolved J coupling to spin B. In addition it must be possible to transfer magnetization from A to C without affecting the spin polarization of B. The accuracy of the measured J value is determined by the accuracy with which peak positions can be determined in a 2D or three-dimensional (3D) spectrum, and by the degree to which the spin polarization of B can be preserved during the experiment. A large number of different schemes based on the ECOSY principle have been proposed for the measurement of homo- and heteronuclear three-bond J couplings.[8-18]

[2] L. J. Smith, M. J. Sutcliffe, C. Redfield, and C. M. Dobson, *Biochemistry* **30,** 986 (1991).
[3] L. E. Kay and A. Bax, *J. Magn. Reson.* **86,** 110 (1989).
[4] F. Delaglio, D. A. Torchia, and A. Bax, *J. Biomol. NMR* **1,** 439 (1991).
[5] M. Billeter, D. Neri, G. Otting, Y. Q. Qian, and K. Wüthrich, *J. Biomol. NMR* **2,** 257 (1992).
[6] S. Ludvigsen, K. V. Andersen, and F. M. Poulsen, *J. Mol. Biol.* **217,** 731 (1991).
[7] C. Griesinger, O. W. Sørensen, and R. R. Ernst, *J. Chem. Phys.* **85,** 6837 (1986).
[8] G. T. Montelione, M. E. Winkler, P. Rauenbühler, and G. Wagner, *J. Magn. Reson.* **82,** 198 (1989).

This chapter focuses on a third category of J coupling measurements, referred to as quantitative J correlation. Although the intensity of a cross-peak has long been used to obtain qualitative information about the magnitude of the active J coupling involved, cross-peak intensity is also influenced by a large number of other factors, including the acquisition times used in the t_1 and t_2 dimensions, the transverse relaxation times of the spins involved, and the magnitude and number of passive J couplings. The quantitative J correlation approach, described below, derives the J value from the intensity ratio between two resonances. Special care is taken that both resonances are affected identically by factors such as relaxation and digitization, and the intensity ratio therefore depends only on the size of the active coupling. A number of different applications of this approach are discussed below.

Measurement of ^1H–^{113}Cd Couplings in Rubredoxin

The first example of quantitative J correlation concerns the measurement of very small ^1H–^{113}Cd J couplings in ^{113}Cd-substituted rubredoxin,[19] a small (5.4 kDa) protein which contains four cysteines ligating the metal in a typical zinc-finger arrangement.[20,21] The pulse scheme used for quantitating the size of the small long-range J couplings between backbone amide protons and ^{113}Cd is sketched in Fig. 1A. In the absence of the ^{113}Cd 180° pulse, all proton magnetization refocuses at the beginning of data acquisition (Fig. 1B). In the presence of the ^{113}Cd 180° pulse, the effect of ^1H–^{113}Cd J coupling is not refocused, and ^1H magnetization vectors coupled to ^{113}Cd in the $|\alpha\rangle$ or $|\beta\rangle$ spin state make angles of $\pm 2\pi J\Delta$

[9] G. Wider, D. Neri, G. Otting, and K. Wüthrich, *J. Magn. Reson.* **85,** 426 (1989).
[10] M. Kurz, P. Schmieder, and H. Kessler, *Angew. Chem., Int. Ed. Engl.* **30,** 1329 (1991).
[11] A. S. Edison, W. M. Westler, and J. L. Markley, *J. Magn. Reson.* **92,** 434 (1991).
[12] R. X. Xu, E. T. Olejniczak, and S. W. Fesik, *FEBS Lett.* **305,** 137 (1992).
[13] M. Sattler, H. Schwalbe, and C. Griesinger, *J. Am. Chem. Soc.* **114,** 1126 (1992).
[14] E. R. P. Zuiderweg and S. W. Fesik, *J. Magn. Reson.* **93,** 653 (1991).
[15] U. Eggenberger, Y. Karimi-Nejad, H. Thüring, H. Rüterjans, and C. Griesinger, *J. Biomol. NMR* **2,** 583 (1993).
[16] S. D. Emerson and G. T. Montelione, *J. Magn. Reson.* **99,** 413 (1992).
[17] G. T. Montelione and G. Wagner, *J. Am. Chem. Soc.* **111,** 5474 (1989).
[18] G. Wagner, P. Schmieder, and V. Thanabal, *J. Magn. Reson.* **93,** 436 (1991).
[19] P. R. Blake, M. F. Summers, M. W. W. Adams, J.-B. Park, Z. H. Zhou, and A. Bax, *J. Biomol. NMR* **2,** 527 (1992).
[20] E. Adman, E. D. Watenpaugh, and L. H. Jensen, *Proc. Natl. Acad. Sci. U.S.A.* **72,** 4854 (1975).
[21] P. R. Blake, J.-B. Park, Z. H. Zhou, D. R. Hare, M. W. W. Adams, and M. F. Summers, *Protein Sci.* **1,** 1508 (1992).

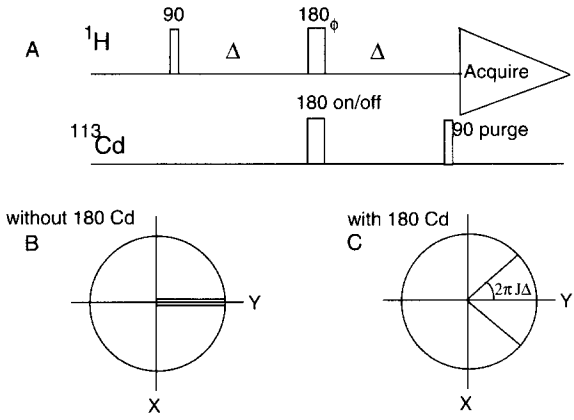

FIG. 1. (A) Pulse sequence used for the quantitative spin-echo difference experiment and positions of ^{1}H magnetization vectors in the transverse plane just prior to the 90° Cd purge pulse in the absence (B) and presence (C) of the ^{113}Cd 180° pulse. To minimize the effects of homonuclear H^N–H^α J couplings, which would decrease the signal-to-noise ratio and add dispersive components to the line shape, the $180°_{\phi_1}$ ^{1}H pulse can be applied as a jump-and-return pulse, $90°_{\phi_1}$–τ–$90°_{-\phi_1}$ This pulse pair, with the ^{1}H carrier positioned on the H_2O resonance and τ set to $1/(2\delta_{HN})$, where δ_{HN} is the frequency difference between carrier and the center of the amide region, then functions as a 180° pulse in the amide region but as a near-zero flip angle pulse in the H^α region. Phase cycling is as follows: $\phi_1 = x, y, -x, -y$; 180° (Cd): 4 scans off, 4 scans on; receiver: $2(x,-x),2(-x,x)$. The reference spectrum, without J modulation, can be obtained using only the first four steps of the phase cycle, that is, with the ^{113}Cd pulse off. For detection of very small J couplings, near-optimal sensitivity in the difference spectrum is obtained when the dephasing delay, Δ, equals the transverse relaxation time of the amide protons.

with the y axis immediately prior to the ^{113}Cd 90° purge pulse (Fig. 1C). The 90° ^{113}Cd purge pulse subsequently transfers the antiphase $\pm x$ magnetization into multiple-quantum coherence, leaving a fraction proportional to $\cos(2\pi J_{HCd}\Delta)$ along the y axis. The ratio of a ^{1}H resonance intensity, measured with and without the ^{113}Cd 180° pulse, is therefore equal to $\cos(2\pi J_{HCd}\Delta)$. In practice, small corrections must be made because the abundance of ^{113}Cd in the sample used is not 100%, and inversion of the ^{113}Cd signal by the 180° pulse in practice is incomplete due to radio frequency (rf) inhomogeneity. However, for $J_{HCd} \ll \Delta^{-1}$ the intensity in the difference spectrum depends quadratically on J_{HCd}, and consequently the measurement is remarkably precise.

The ^{1}H–{^{113}Cd} spin-echo difference spectrum, recorded at a ^{1}H frequency of 600 MHz with a Δ duration of 70 msec, is shown in Fig. 2B. Besides the intense H^β resonances of the cysteine residues coordinating the Cd atom, the difference spectrum also shows resonances of five back-

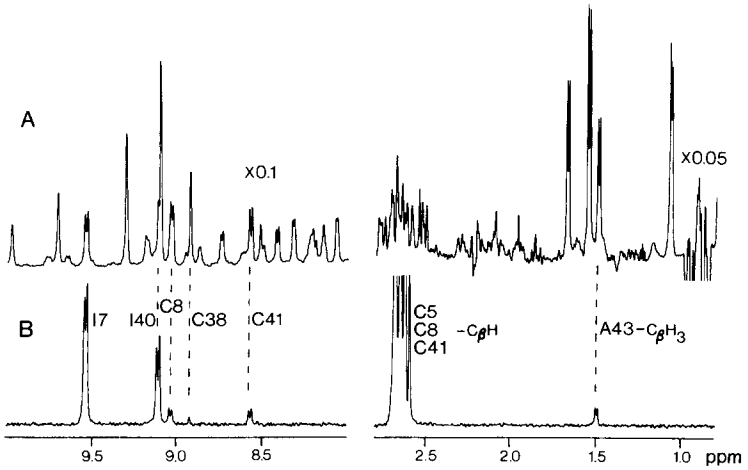

FIG. 2. Selected regions of the ^{1}H NMR spectrum of ^{113}Cd-substituted rubredoxin, acquired with the ^{1}H–{^{113}Cd} spin-echo difference experiment of Fig. 1, using Δ = 70 msec. (A) Spectrum obtained using the first four steps of the phase cycle, that is, without affecting the ^{113}Cd spin state. The spectrum results from 1200 transients. (B) Spectrum obtained using the full eight-step phase cycle spin-echo difference experiment with parameters identical compared to (A) except for the number of transients (60,000 with Cd 180°, and 60,000 without Cd 180°). The total measuring time was approximately 36 hr. The downfield and upfield regions of the ^{1}H spectrum shown in (A) are displayed at 5- and 2.5-fold higher magnification compared to (B), 0.1- and 0.05-fold after correction for the number of transients. J modulation is suppressed in the downfield region of the spectrum but causes a noiselike appearance of the baseline in the upfield reference spectrum; signal-free baseline in the upfield region is visible only near the methyl resonance at 1.1 ppm. (From Blake *et al.*[19])

bone amide protons and, most remarkably, of the methyl protons of an alanine residue.[19,22] Four of the five amide protons are hydrogen bonded to the sulfur atoms coordinating the Cd atom.[20,21] The small (0.3 Hz) J coupling to the fifth amide (Cys-38) is presumably a regular five-bond coupling. Both the solution and the crystal structure show that the methyl group of Ala-43 is in very close proximity to the sulfur atom of Cys-41, and the J coupling to Ala-43–C$^\beta$ H_3 presumably is caused by a small degree of orbital overlap.

The spectra recorded with and without the ^{113}Cd 180° pulse are affected by identical relaxation effects, but with one exception: ^{113}Cd spin flips during the 2Δ period would inhibit dephasing of the two proton vectors, thereby attenuating the difference spectrum and resulting in an underesti-

[22] P. R. Blake, J.-B. Park, M. W. W. Adams, and M. F. Summers, *J. Am. Chem. Soc.* **114,** 4931 (1992).

mate for J_{HCd}. Considering that coordination of the metal is nearly tetrahedral,[20,21] the chemical shift anisotropy (CSA) of the Cd nucleus should be small. As CSA is the dominant relaxation mechanism for ^{113}Cd, the ^{113}Cd T_1 is expected to be long, and the effect of ^{113}Cd spin flips is negligible in this particular application of quantitative J correlation.

Measurement of H^β to Backbone Amide and Carbonyl J Couplings

Coupling between the backbone amide and H^β protons provides information about the χ_1 torsion angle. Similar information can be obtained from the coupling between H^β and the backbone carbonyl. In fact, these two measurements complement one another, and together they can frequently determine the χ_1 angle and the stereospecific assignment of the H^β protons in an unambiguous manner. The experiment for measurement of the ^{15}N–$^1H^\beta$ coupling relies on quantitating the fraction of magnetization transferred from ^{15}N to H^β, and vice versa, in a 3D spectrum that correlates intraresidue H^N, N, and H^β resonances. This type of correlation is referred to as an HNHB experiment (Fig. 3). The complementary HN(CO)HB

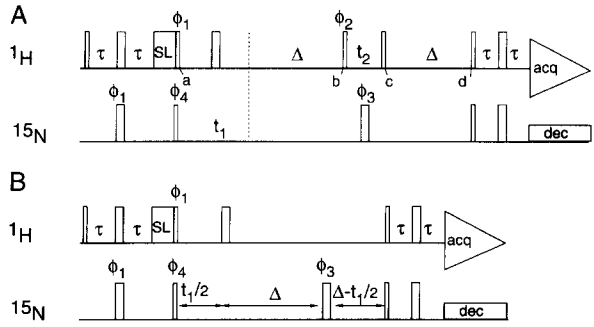

FIG. 3. Pulse scheme of the HNHB experiment (A) for obtaining the 3D spectrum containing the H^N–H^β long-range correlations and (B) for obtaining a 2D ^1H–^{15}N spectrum containing the reference intensity information. Narrow and wide pulses have flip angles of 90° and 180°, respectively. The pulse labeled SL corresponds to a 1-msec spin-lock pulse for H_2O suppression. Pulses for which no rf phase is indicated are applied along the x axis. Phase cycling is as follows: $\phi_1 = y,-y$; $\phi_2 = 8(x),8(-x)$; $\phi_3 = 2(x),2(y),2(-x),2(-y)$; $\phi_4 = x$; receiver: $2(x,-x,-x,x),2(-x,x,x,-x)$. For the reference spectrum (B), only the first eight steps of the above phase cycle are used. For both experiments, quadrature in the t_1 dimension is used by incrementing ϕ_4 in the usual States–TPPI (time-proportional phase incrementation) manner. For obtaining quadrature in the t_2 dimension of the 3D experiment, ϕ_2 is incremented in the States–TPPI manner. Delay durations are $\tau = 2.25$ msec; $\Delta = 27$ msec.

experiment (Fig. 4) correlates the amide proton and ^{15}N resonances of residue i with the H^{β} of residue $i-1$. In this experiment magnetization is first transferred from the amide proton via its nitrogen to the preceding carbonyl, which is then J correlated with its intraresidue H^{β} protons, followed by magnetization transfer in the reverse direction, from carbonyl to H^N. In this experiment, the intensity of the correlation is a function of the three-bond H^{β}–CO J coupling.

Detailed descriptions of the HNHB and HN(CO)HB experiments, when used in a qualitative fashion, have been provided by Archer *et al.*[23] and Grzesiek *et al.*,[24] respectively. Because the two experiments are conceptually identical to one another, only a brief qualitative discussion of the HNHB experiment is presented below. In this pulse scheme H^N magnetization is transferred into antiphase ^{15}N–$\{^1H^N\}$ magnetization by the insensitive nucleus enhancement by polarization transfer (INEPT) method at time a. After an ^{15}N evolution period, t_1, ^{15}N magnetization dephases owing to J coupling with protons that have a long-range interaction with this ^{15}N. If the dephasing delay Δ is set to an odd multiple of $1/(2J_{NH})$, where J_{NH} is the one-bone ^1H–^{15}N J coupling (~92 Hz), the ^{15}N has rephased with respect to its directly attached proton at the end of the first Δ interval but will have partially dephased owing to long-range coupling (J_{NB}) to a proton H^B ($H^B = H_i^{\beta 2}$, $H_i^{\beta 3}$, H_i^{α}, or H_{i-1}^{α}). The subsequent $90°_{\phi_2}$ ^1H pulse converts the antiphase $N_y H^B_z$ magnetization to $N_y H^B_y$ multiple-quantum coherence, which is converted back to $N_y H^B_z$ magnetization at the end of the H^B evolution period, t_2. At the end of the second Δ interval, $N_y H^B_z$ magnetization has partially rephased with respect to H^B and completely dephased with respect to its attached amide proton. A subsequent reverse INEPT, applied at time d, converts this magnetization to the observed amide proton magnetization. It is easily shown that the integrated intensity of an H^N–H^B correlation is proportional to

$$\sin^2(\pi J_{NB}\Delta) \prod_{k \neq B} \cos^2(\pi J_{Nk}\Delta) \exp(-2\Delta/T_{2N}) \qquad (1)$$

where the product extends over all protons, k, other than B that have a long-range interaction with N, and T_{2N} is the ^{15}N transverse relaxation time in the absence of ^1H decoupling. Previously, the H^N–H^{β} J coupling, J_{NB}, was estimated qualitatively from the intensity of the correlation in the 3D HNHB spectrum.[23] The J_{NB} value can be determined quantitatively if a reference 2D spectrum is recorded, as sketched in Fig. 3B.

[23] S. J. Archer, M. Ikura, D. A. Torchia, and A. Bax, *J. Magn. Reson.* **95,** 636 (1991).
[24] S. Grzesiek, M. Ikura, G. M. Clore, A. M. Gronenborn, and A. Bax, *J. Magn. Reson.* **96,** 215 (1992).

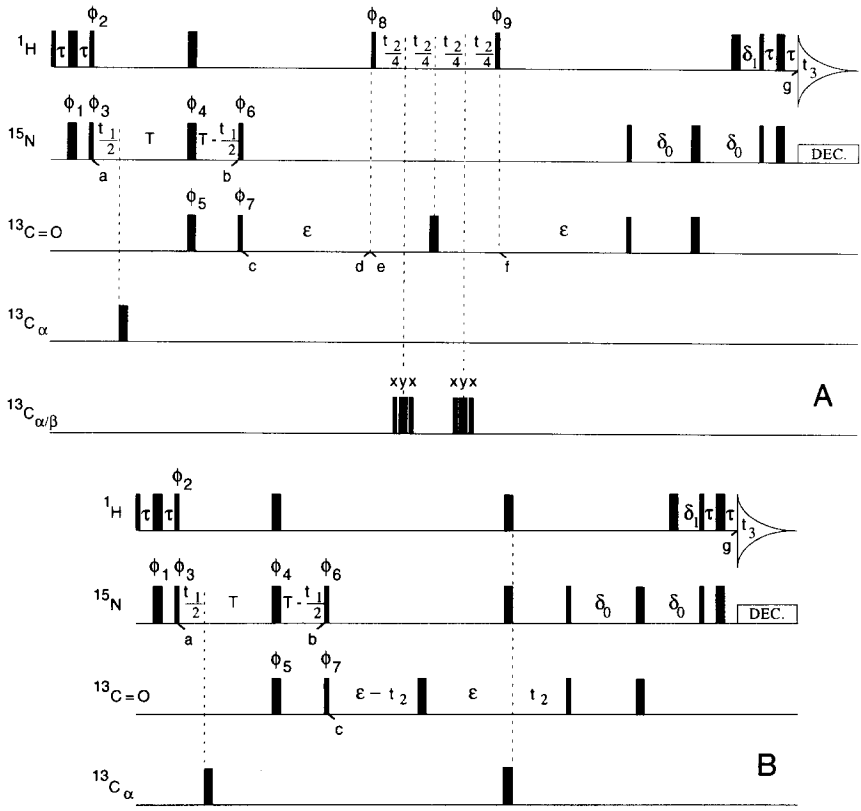

FIG. 4. Pulse scheme of (A) the 3D HN(CO)HB experiment and (B) the 3D reference constant-time (t_1/t_2) 3D HNCO experiment. Narrow and wide pulses correspond to 90° and 180° flip angles, respectively. Pulses for which the phase is not indicated are applied along the x axis. Phase cycling of the other pulses is as follows: (A) $\phi_1 = x,-x$; $\phi_2 = y,-y$; $\phi_3 = x$; $\phi_4 = 4(x),4(y),4(-x),4(-y)$; $\phi_5 = 16(x),16(-x)$; $\phi_6 = 8(x),8(-x)$; $\phi_7 = x,x,-x,-x$; $\phi_8 = 16(x),16(-x)$; $\phi_9 = 4(x),8(-x),4(x)$; Acq. $= 4(x,-x,-x,x)$, $4(-x,x,x,-x)$; (B) $\phi_1 = x,-x$; $\phi_2 = y,-y$; $\phi_3 = x$; $\phi_4 = 4(x),4(y),4(-x),4(-y)$; $\phi_5 = 16(x),16(-x)$; $\phi_6 = 8(x),8(-x)$; $\phi_7 = x,x,-x,-x$; Acq. $= x,-x,-x,x,-x,x,x,$ $-x,-x,x,x,-x,x,-x,-x,x$. For both schemes, quadrature in the t_1 dimension is obtained by altering ϕ_3 in the usual States–TPPI manner. Quadrature in the t_2 dimension is obtained by changing ϕ_8 (A) and ϕ_7 (B) in the States–TPPI manner. Delay durations are as follows: $\tau = 2.25$ msec; $T = 13.5$ msec; $\varepsilon = 25$ msec; $\delta_0 = 10$ msec; $\delta_1 = 2.75$ msec. The C^α pulse is applied with the carrier at 56 ppm, $C^{\alpha/\beta}$ pulses with the carrier at 44.5 ppm. For both C^α and $C^{\alpha/\beta}$ pulses, the rf power is adjusted to give a null in the excitation profile in the carbonyl region.

The *integrated* intensity of a ^1H–^{15}N correlation in the 2D ^1H–^{15}N reference spectrum depends in the same way on the $^1H^N$ and ^{15}N transverse relaxation rates as does the intensity of the H^N–N–H^β correlation in the 3D spectrum. The intensity ratio of the volume integral of the H^N–N–H^β correlation (V_{HNB}) in the 3D spectrum and the volume integral (V_{HN}) of the H^N–N correlation in the 2D reference spectrum is therefore given by

$$V_{HNB}/V_{HN} = \sin^2(\pi J_{NB}\Delta) \prod_{k \neq B} \cos^2(\pi J_{Nk}\Delta) \quad (2)$$

This ratio applies to the case where the number of scans per increment is identical for the 2D and 3D experiments. Although at first sight it may appear unusual to compare integrals from 2D and 3D spectra, the integral of a resonance in a 2D or 3D spectrum by definition corresponds to the value of the corresponding time domain component at time zero. This value is independent of the dimensionality of the pulse scheme, that is, independent of whether a given delay is fixed or systematically incremented as a variable evolution period. In practice, most discrete Fourier transformation programs do not scale for the number of data points used in the transform. Before comparing volume integrals it is therefore necessary to divide the volume integral by $N_1 \times N_2/4$ for the 2D case and by $N_1 \times N_2 \times N_3/8$ for the 3D case, where N_1, N_2, and N_3 are the number of real data points after Fourier transformation in the F_1, F_2, and F_3 dimension, respectively.[25]

As can be seen from Eq. (2), the volume ratio is affected not only by the coupling of interest, J_{NB}, but also by passive couplings J_{Nk}. For cases where $\Delta \ll 1/2J_{Nk}$, the effect of the cosine terms in Eq. (2) is very small. If this condition does not apply, J_{Nk} will give rise to a sizable correlation between the ^{15}N nucleus and proton k, and the J couplings can be determined by considering simultaneously the intensities of all cross-peaks to a given amide.

Figure 5 shows F_2 strips through the HNHB and HN(CO)HB spectra of the protein calmodulin complexed with a 26-residue peptide fragment of myosin light chain kinase. Clearly, measurement of both the $^1H^\beta$–^{15}N and $^1H^\beta$–^{13}CO J couplings allows, in many cases, unambiguous assignment of the diastereotopic H^β protons and yields the side-chain torsion angle χ_1. Although in principle this information can be derived from a qualitative interpretation of the heteronuclear J couplings, quantitative J values are strongly preferred because they can identify the presence of rotameric averaging.

[25] G. W. Vuister, T. Yamazaki, D. A. Torchia, and A. Bax, *J. Biomol. NMR* **3**, 297 (1993).

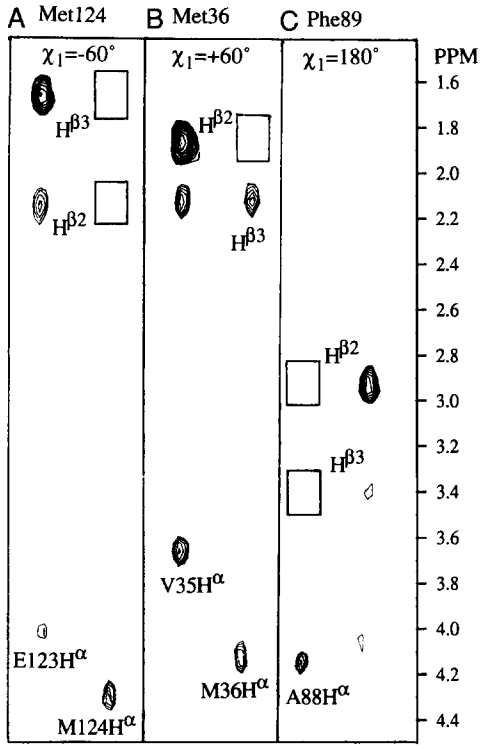

FIG. 5. Strips taken from the 3D HNHB spectrum (left-hand side) and the corresponding strips from the HN(CO)HB (right-hand side) spectrum of calmodulin, complexed with a 26-residue peptide. HNHB strips have been selected at the ^{15}N–^{1}H (F_1,F_3) frequencies of the amides of (A) Met-124, (B) Met-36, and (C) Phe-89; HN(CO)HB strips are taken at the ^{15}N–^{1}H (F_1,F_3) frequencies of the amides of Ile-125, Arg-37, and Arg-90, displaying J correlation via its preceding carbonyl to the side chain of the preceding residue. The intensity of each correlation is related to the size of the J coupling [cf. Eq. (2)]. The fact that the correlations to the carbonyl are less intense than those to the backbone ^{15}N reflects the fact that the inherent sensitivity of the HN(CO)HB experiment is lower than for the HNHB experiment, owing to the additional dephasing and rephasing intervals.

Measurement of Three-Bond ^{13}C–^{13}C J Couplings

The ^{13}C–^{13}C three-bond J couplings are important carriers of structural information, and a dihedral Karplus relationship for this coupling is well established.[26] In ^{13}C-enriched proteins, direct measurement of $^{3}J_{CC}$ values is generally not possible because of the small magnitude of the couplings (0–4 Hz) relative to the ^{13}C line width, and because any given ^{13}C reso-

[26] L. V. Krivdin and E. W. Della, *Prog. Nucl. Magn. Reson. Spectrosc.* **23**, 301 (1991).

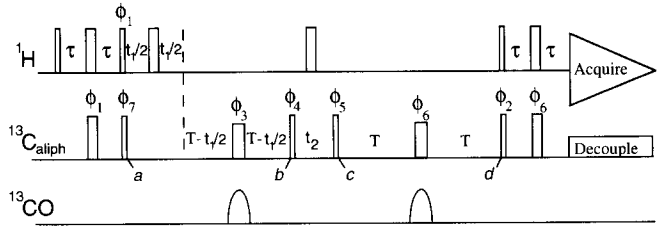

FIG. 6. Pulse scheme of the 3D version of the ^{1}H-detected quantitative [^{13}C–^{13}C] long-range correlation experiment. Narrow and wide pulses correspond to flip angles of 90° and 180°, respectively. All ^{13}C pulses are applied at the highest possible power level, except for the 180°$_{\phi_3}$ and 180°$_{\phi_6}$ pulses. For the 180°$_{\phi_3}$ and 180°$_{\phi_6}$ pulses the power is reduced to yield a null in the excitation profile at the carbonyl frequency. Shaped pulses applied to the carbonyl spins have a 180° flip angle and do not excite the aliphatic ^{13}C spins. Phase cycling: $\phi_1 = y,-y$; $\phi_2 = 2(y),2(-y)$; $\phi_3 = 2(x),2(-x),2(y),2(-y)$; $\phi_4 = 8(x),8(-x)$; $\phi_5 = 16(x)$, $16(-x)$; $\phi_6 = x$; $\phi_7 = y$; receiver: $x,2(-x),x,-x,2(x),-x$. Quadrature in the t_1 and t_2 dimensions is obtained by changing ϕ_7 and ϕ_4, respectively, in the usual States–TPPI manner.

nance is frequently split by half a dozen or more one-, two, and three-bond J_{CC} couplings. The line width problem is alleviated for methyl groups that experience reduced heteronuclear dipolar broadening because of rapid rotation about their 3-fold symmetry axis. In addition, because of cross-correlation effects, the transverse relaxation of methyl carbons in proteins is highly nonexponential, and the slowly decaying component of the $^{13}CH_3$ magnetization gives rise to a spectral component with a width of only a few hertz, even in proteins as large as 20 kDa. This slowly relaxing transverse methyl magnetization can be used to generate an "in-phase" ^{13}C–^{13}C correlation spectroscopy (COSY) spectrum in a manner briefly outlined below. As is the case for the experiments described above, the intensity of the observed correlation between the methyl carbon and other carbons again depends, to first order, quadratically on the size of the mediating J coupling.

The pulse scheme for the ^{13}C–^{13}C correlation experiment[27] is shown in Fig. 6. It can be conducted either as a 2D experiment, by keeping $t_1 = 0$, or as a 3D experiment. The 2D version is briefly described below. The 2D and 3D versions differ only by the fact the first dephasing period between time points a and b of the 2D version is converted to a constant-time ^{13}C evolution period in the 3D experiment. The ^{1}H magnetization is transferred via an INEPT sequence to its directly attached ^{13}C nucleus (time a). During the subsequent dephasing period, of total duration $2T$, dephasing caused by both $^1J_{CC}$ and $^nJ_{CC}$ takes place. The ^{13}C chemical

[27] A. Bax, D. Max, and D. Zax, *J. Am. Chem. Soc.* **114,** 6924 (1992).

shifts are refocused during this period by the application of a 180° ^{13}C pulse, applied at the midpoint of the interval. Because at high magnetic field strengths it is difficult to generate a single 180° pulse that simultaneously inverts the entire 170 ppm ^{13}C bandwidth, the rectangular 180° pulse is applied at reduced power such that its excitation profile has a null in the carbonyl region, and it is followed immediately by a shaped 180° carbonyl inversion.

The duration of $2T$ is set to $1/^1J_{CC}$ (29 msec), such that at time b the dephasing caused by $^1J_{CC}$ is near zero. However, a long-range coupling J^n_{CC} to carbon n causes dephasing proportional to $\sin(2\pi J^n_{CC}T)$. The resulting antiphase methyl magnetization at time b is converted to antiphase magnetization of its coupling partner, n, by the subsequent $90°_{\phi_4}$ pulse. After a short t_1 evolution period (0–8 msec), the antiphase magnetization of spin n is converted back to antiphase methyl transverse magnetization at time c. After another $2T$ refocusing period (at time d), a fraction $\sin(2\pi J^n_{CC}T)$ of methyl magnetization, antiphase with respect to spin n at time c, will have refocused and is subsequently transferred back to the methyl protons for detection. In the 2D spectrum, the methyl proton resonance therefore shows a correlation to the long-range coupled carbon with an integrated intensity proportional to $-\sin^2(2\pi J^n_{CC}T)\,\Pi_{m\neq n}\cos^2(2\pi J^m_{CC}T)$, and a correlation to its directly attached carbon with an intensity proportional to $\Pi_m \cos^2(2\pi J^m_{CC}T)$, where J^m_{CC} denotes the coupling between the methyl carbon and other carbons, m. Therefore the ratio of the integrated peak volumes of the correlations to the long-range coupled carbon n and to the methyl carbon equals $-\tan^2(2\pi J^n_{CC}T)$.

Figure 7 shows three regions of the quantitative ^{13}C–^{13}C long-range correlation spectrum obtained for the protein calmodulin complexed with the 26-residue peptide mentioned above. Figure 7B contains the "diagonal" ^{13}C methyl resonances corresponding to magnetization not transferred to any of its long-range coupling partners at time b in the scheme of Fig. 6. Figure 7C contains correlations to C^α carbons. For example, the most upfield shifted proton resonance at 0.3 ppm, corresponding to the C^δ methyl protons of Leu-32, shows a correlation to its attached ^{13}C in Fig. 7B. In Fig. 7C, plotted at a 10-fold lower contour level, a correlation to the Leu-32–C^α resonance is observed. The relative intensity of the two resonances reveals a C^δ–C^α J coupling of 3.3 Hz, indicative of a trans conformation.

Figure 7A shows long-range correlations to the carbonyl resonances. Both the Val-142 C^γ $^1H_3$ (0.74 ppm) and $C^{\gamma 2}H_3$ (0.50 ppm) resonances show correlations to the Val-142 carbonyl (at 179.6 ppm). However, the $C^{\gamma 2}$ correlation is much stronger than the $C^{\gamma 1}$ correlation, and the J couplings derived from the intensity ratios are 1.0 and 2.5 Hz, respectively.

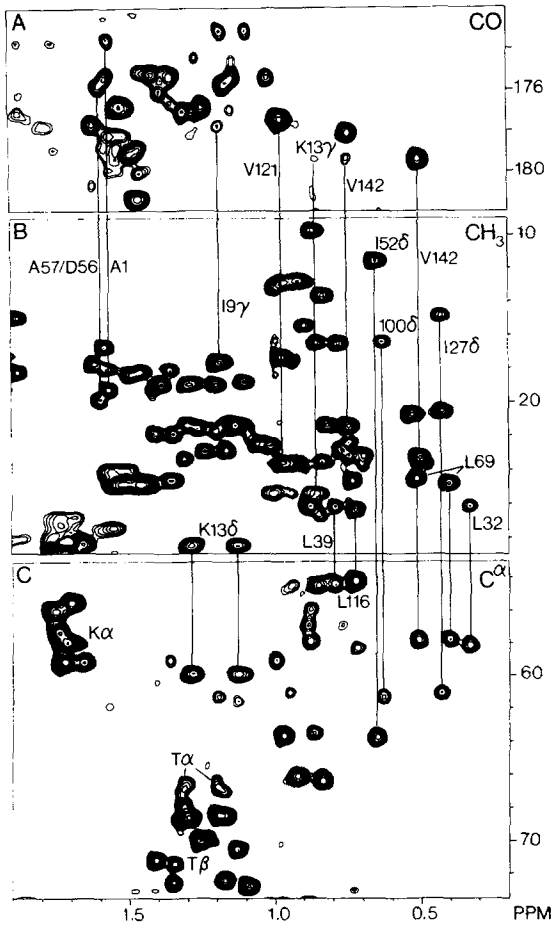

FIG. 7. The ^{1}H-detected 2D quantitative ^{13}C–^{13}C long-range correlation spectrum of ^{13}C-enriched calmodulin, complexed with a 26-residue peptide. The methyl region (B) corresponds to magnetization not transferred via long-range couplings. Correlations to the carbonyls are shown in (A) and correlations to the C^{α} region in (C). The methyl region is plotted at a contour level 10 times higher than the cross-peak regions, and resonances in (B) are opposite in sign relative to (A) and (C). The intensity of the overlapping signals in the methyl region is obtained from a high-resolution reference ^{1}H–^{13}C spectrum, recorded with a constant-time evolution period set to $4T$. For all resonances resolved in (B), a very good proportionality between the integrated intensity in the low-resolution display of (B) and the high-resolution reference spectrum was established, thus yielding accurate intensities for methyl resonances that are overlapping in (B) but resolved in the reference spectrum. The spectrum was recorded on a Bruker AMX-600 spectrometer, and the total accumulation times were 7.5 hr for the spectrum shown and 2 hr for the reference spectrum. (From Bax *et al.*[27])

The correlations in Fig. 7B are the least resolved, and this leads to problems when attempting to measure peak intensities. Note that this overlap problem is not resolved by conducting the experiment in a 3D fashion. Instead, a reference spectrum is obtained from a constant-time ^1H–^{13}C heteronuclear single-quantum coherence (CT-HSQC) spectrum,[28] with the duration of the constant-time evolution period set to 58 msec (corresponding to $4T$ in Fig. 6). The resolution in such a constant-time HSQC spectrum is much higher and allows the intensities of most methyl correlations to be measured. For resonances resolved in Fig. 7B, a single proportionality constant is found relative to the intensities in the CT-HSQC spectrum. Using this proportionality constant, intensities of methyl resonances overlapping in Fig. 7B are determined from the better resolved CT-HSQC spectrum.

Coupling constants derived directly from the $\tan^2(2\pi^n J_{CC}T)$ intensity ratio, mentioned above, are expected to be systematically smaller than the true coupling. This systematic difference is caused primarily by rf inhomogeneity and rf offset effects. For example, if in an extreme case the $90°_{\phi_4}$ and $90°_{\phi_5}$ pulses were reduced in effective flip angle to 45° because of off-resonance effects, this would result in a 2-fold reduction in intensity and a reduction by $2^{1/2}$ in the size of the derived coupling. However, provided that strong rf fields are used and rf homogeneity is good, the systematic error tends to be much smaller (of the order of 10% or less).

Measurement of Three-Bond ^{13}C–^{15}N Couplings

Three-bond ^{13}C–^{15}N J couplings to the backbone amide ^{15}N are even smaller than ^{13}C–^{13}C J couplings to the backbone carbonyl, and historically they have been very difficult to measure. Recently, however, a two-dimensional spin-echo difference experiment has been described that makes it possible to quantitate this coupling, even in proteins as large as 20 kDa.[29] As was the case for measurement of $^3J_{CC}$ described above, only couplings to methyl carbons can be measured for proteins in this molecular weight range. Despite this limitation, the simple experiment described below, together with knowledge of the ^{13}C–^{13}C coupling to the backbone carbonyl, provides the stereospecific assignment of Val methyl resonances as well as the χ_1 angle in Val, Ile, and Thr residues. Methyl groups of these residues are frequently involved in long-range nuclear Overhauser effect (NOE) interactions, and accurate knowledge of the χ_1 angle (and

[28] G. W. Vuister and A. Bax, *J. Magn. Reson.* **98,** 428 (1992).
[29] G. W. Vuister, A. Wang, and A. Bax, *J. Am. Chem. Soc.* **115,** 5334 (1993).

stereoassignments for Val) can significantly improve the precision with which the interior of a protein structure can be defined.

The pulse scheme (Fig. 8) is a 2D analog of the simple 1D spin-echo difference experiment of Fig. 1. When the ^{15}N 180° pulse is applied in position a, the scheme is identical to the constant-time ^{1}H–^{13}C correlation experiment (CT-HSQC), described elsewhere.[29] The effect of one-bond ^{13}C–^{13}C J couplings during the constant-time evolution period is again suppressed by adjusting the duration ($2T$) of the constant-time evolution period to $2/^{1}J_{CC}$ (58 msec). The effect of ^{13}C–^{15}N J coupling is eliminated by the 180° pulse applied at position a. In the second experiment, the 180° ^{15}N pulse is shifted to position b, causing the J_{CN} coupling to be active during the entire $2T$ period. In the latter case, ^{13}C magnetization is attenuated by $\cos(2\pi J_{NC}T)$ relative to the scheme with the 180° pulse in position a. The two experiments are executed in an interleaved manner with the results stored separately. Subtraction of the results gives a relative intensity of $1 - \cos(2\pi J_{NC}T) = 2\sin^2(\pi J_{NC}T)$ in the difference spectrum, allowing J_{NC} to be calculated straightforwardly.

The methyl region of the ^{13}C–{^{15}N} spin-echo difference CT-HSQC spectrum of calmodulin, complexed with the 26-residue peptide fragment, is shown in Fig. 9. As can be seen, all eight calmodulin Ile $C^{\gamma 2}$ methyl carbons are present. From the intensities in the difference spectrum, the

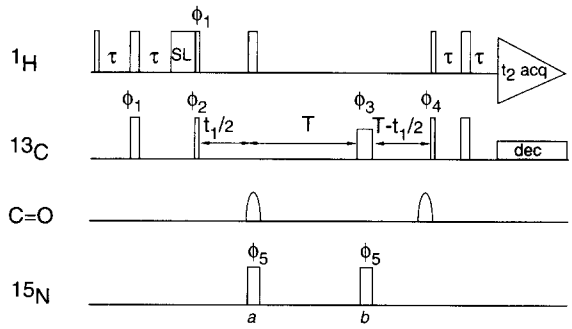

FIG. 8. Pulse scheme for the ^{13}C–{^{15}N} spin-echo difference CT-HSQC experiment. Narrow and wide pulses denote 90° and 180° flip angles, respectively. The power of the $180°_{\phi_3}$ pulse is adjusted to avoid excitation of the carbonyl resonance. Further details are described elsewhere.[28] The reference CT-HSQC experiment is recorded using the ^{15}N pulse labeled a and omitting the pulse labeled b, whereas the attenuated CT-HSQC experiment is recorded using pulse b and omitting pulse a. Unless indicated otherwise, all pulses are applied along the x axis. The phase cycle is as follows: $\phi_1 = y,-y$; $\phi_2 = x$; $\phi_3 = 2(x),2(-x),2(y),2(-y)$; $\phi_4 = 8(x),8(-x)$; $\phi_5 = 16(x),16(-x)$; receiver: $2(x,-x),4(-x,x),2(x,-x)$. Phase ϕ_2 is incremented to achieve quadrature detection in t_1 in the usual States–TPPI manner. The delays τ and T were set to 1.7 and 28.6 msec, respectively.

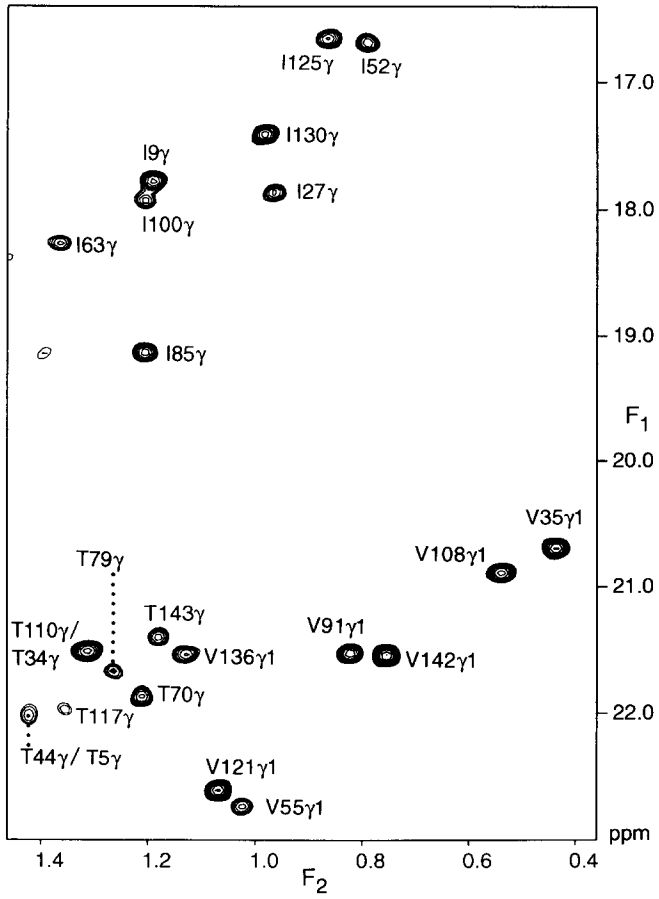

FIG. 9. Methyl region of the ^{13}C–{^{15}N} spin-echo difference CT-HSQC spectrum of calmodulin, complexed with a 26-residue peptide. The two spectra from which the difference spectrum is calculated have been recorded in an interleaved manner, with acquisition times of 51 msec (t_1) and 53 msec (t_2) and spectral widths of 33 ppm (F_1,^{13}C) and 8 ppm (F_2,^1H). Spectra were recorded at 35° on a Bruker AMX-600 spectrometer with a total measuring time of 17 hr. (From Vuister and Bax.[28])

corresponding couplings are calculated to fall in the range 1.8 (Ile-130) to 2.1 Hz (Ile-27), indicating that they are all in a trans orientation relative to the intraresidue ^{15}N. Therefore, all eight Ile residues have χ_1 angles of $-60°$. This conformation is confirmed by small couplings between the $C^{\gamma 2}$ and the carbonyl carbon for all eight Ile residues.[27] For each of the seven valines, only one of the two diastereotopic methyl carbons is observed in the difference spectrum. For example, at a ^1H frequency of 0.75 ppm

the resonance of one of the two C^{γ} methyl resonances of Val-142 shows a resonance intensity in the ^{13}C–$\{^{15}N\}$ spin-echo difference CT-HSQC spectrum (Fig. 9) that corresponds to a $^3J_{NC^{\gamma}}$ value of 1.8 Hz. No resonance in the difference spectrum is observed for the second methyl carbon of Val-142 (at $^1H/^{13}C$ shifts of 0.50/23.2 ppm), indicating that its coupling to the backbone ^{15}N must be smaller than 0.7 Hz. Together with C^{γ}–CO J couplings of 1 Hz for the 0.75 ppm resonance and 2.5 Hz for the 0.50 ppm methyl resonance (Fig. 7), this immediately identifies the resonance at 0.74 ppm as $C^{\gamma 1}H_3$ and the one at 0.50 ppm as $C^{\gamma 2}H_3$. These couplings also unambiguously determine the χ_1 angle to be 180°. In fact, for six of the seven calmodulin valine residues, the $^3J_{C^{\gamma}N}$ couplings together with $^3J_{C^{\gamma}CO}$ values indicate χ_1 angles of 180°. For Val-55, however, $^3J_{C^{\gamma 1}N}$ is smaller than for the other residues (1.2 Hz). Moreover, its $C_{\gamma 1}$ also shows a 1.7 Hz coupling to the carbonyl, indicating rotamer averaging between $\chi_1 = 180°$ and $\chi_1 = -60°$. As can be seen from this example, the high precision with which the very small ^{13}C–^{13}C and ^{13}C–^{15}N J couplings can be measured is extremely valuable for the identification of residues that are subject to χ_1 rotamer averaging. For Val-55, slow conformational averaging had previously been noted on the basis of its anomalously short ^{15}N T_2 value,[30] but the nature of the conformational rearrangement had been unclear.

In addition to yielding the magnitude of the $^3J_{CN}$ coupling constants, the experiment described here is also useful for identification of Pro $C^{\delta}H_2$, Lys $C^{\epsilon}H_2$, Arg $C^{\delta}H_2$, Gln $C^{\gamma}H_2$, and Asn $C^{\beta}H_2$ resonances, which are of high intensity in the 2D difference spectrum because of the substantial $^1J_{CN}$ and $^2J_{CN}$ coupling to the adjacent nitrogen.

Measurement of $^3J_{CH}$ Couplings to Methyl Carbons

Above, the long transverse relaxation time of a fraction of the methyl ^{13}C magnetization has been exploited for the measurement of $^3J_{CC}$ and $^3J_{CN}$ couplings. It has been shown that the same characteristic can also be used to measure ^1H–^{13}C long-range couplings. Although the experiment is conducted most effectively for samples in which the methyl groups have been enriched selectively with ^{13}C,[25] it can also be applied to proteins uniformly enriched with ^{13}C; the discussion below is restricted to this latter application.[31]

The pulse scheme for quantitative ^1H–^{13}C long-range correlation, known as LRCH (long-range CH correlation) is shown in Fig. 10. Concep-

[30] G. Barbato, M. Ikura, L. E. Kay, and A. Bax, *Biochemistry* **31,** 5269 (1992).
[31] G. W. Vuister and A. Bax, *J. Magn. Reson. Ser. B* **102,** 228 (1993).

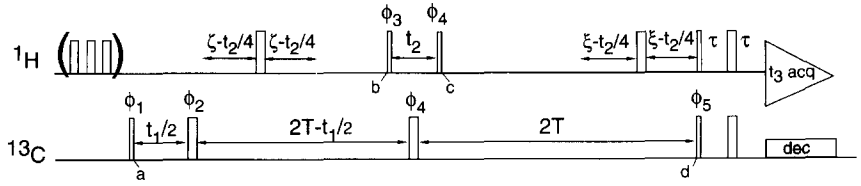

FIG. 10. Pulse sequence of the 3D ^{1}H-detected quantitative [^{13}C–^{1}H] long-range correlation experiment, applicable to proteins uniformly enriched in ^{13}C. Narrow and wide pulses correspond to 90° and 180° flip angles, respectively. Unless indicated otherwise, all pulses are applied along the x axis. The phase cycle is as follows: $\phi_1 = x; \phi_2 = 4(x),4(y),4(-x),4(-y)$; $\phi_3 = x,-x$; $\phi_4 = 2(x),2(-x)$; $\phi_5 = 16(y),16(-y)$; receiver: $P,-P,P,-P,-P,P,-P,P$, with $P = (x,-x,-x,x)$. The 2D reference spectrum is recorded by setting $t_2 = 0$, and using $P = 4(x)$ for the receiver phase. Quadrature detection in t_1 and t_2 is obtained with the States–TPPI technique by incrementing phases ϕ_1 and ϕ_3, respectively. The pulse train on the ^{1}H channel during the relaxation delay consists of low-power 135° pulses, spaced by 10 msec delays, and serves to build up the heteronuclear NOE. Delay durations are τ = 1.7 msec, $2T$ = 29.6 msec, ζ = 3 msec, and ξ = 4 msec, permitting a maximum acquisition time in the t_2 dimension of 12 msec. (From Vuister and Bax.[31])

tually it is related closest to the HNHB and HN(CO)HB experiments of Fig. 3 and 4. The main difference results from the fact that in the present experiment, additional care must be taken to avoid interference from large one-bond ^{1}H–^{13}C and ^{13}C–^{13}C J couplings. A brief description of the LRCH experiment is given below.

Figure 10 is essentially an "inverted" HMQC-type experiment. The ^{13}C methyl magnetization starts on ^{13}C and the $90°_{\phi_3}$ ^{1}H pulse converts the ^{13}C transverse magnetization to ^{1}H–^{13}C zero- and double-quantum coherence. The $180°_{\phi_4}$ pulse interconverts the zero- and double-quantum coherence components, causing the signal to be t_2-modulated by the frequency of the ^{1}H chemical shift. At the end of the t_2 evolution period, the multiple-quantum coherence is transferred back into transverse ^{13}C magnetization by the $90°_{\phi_4}$ ^{1}H pulse, and, after a suitable refocusing period, ^{13}C methyl magnetization is transferred to its directly attached protons by means of a reverse INEPT just prior to ^{1}H detection. The LRCH scheme starts with an NOE enhancement of ^{13}C instead of with the more common INEPT transfer in order to avoid generation of unwanted antiphase components at the end of the first $2T$ period. For methyl groups, this is not a significant disadvantage as the NOE enhancement is typically around 2.5, and ^{13}C T_1 relaxation is quite rapid. To avoid interference of $^1J_{CC}$ couplings, the time between the $90°_{\phi_1}$ and $90°_{\phi_5}$ pulses must be kept constant at $2/^1J_{CC}$ (58 msec, in practice). The effect of ^{13}C dephasing caused by the $^1J_{CH}$ interaction is eliminated by ensuring that the duration for which $^1J_{CH}$ is active (between time points a and b) equals a multiple of $1/^1J_{CH}$. These

two requirements can be satisfied simultaneously by separating the $180°_{\phi_2}$ ^{13}C pulse and the first ^{1}H 180° pulse by a t_2-dependent duration, $\zeta - t_2/4$. This means that $^{13}C\{-^{1}H\}$ dephasing between time points a and b is active for a total time of $2T - 2\zeta$ (23.6 msec). Rephasing, between time points c and d, is active for a time $2T - 2\xi$, which is set 2 msec shorter than $3/^{1}J_{CH}$ in order to generate ^{13}C magnetization antiphase with respect to a single methyl proton, prior to the reverse INEPT at time point d.

The easiest way to quantitate the fraction of ^{13}C magnetization transformed into heteronuclear multiple-quantum coherence at time b is to record a 2D reference spectrum by keeping $t_2 = 0$, and by using the phase cycling indicated in the legend to Fig. 10. As discussed above for the HNHB and HN(CO)HB experiments, integrated intensities in the 2D and 3D spectra are directly related but require normalization to account for the different dimensionalities.[25] The ratio of the volume of a long-range correlation to a proton i in the 3D spectrum, V_{3D}, to the integral of the corresponding $^{13}C-^{1}H_3$ correlation in the reference spectrum, V_{2D}, is given by

$$\begin{aligned} V_{3D}/V_{2D} &= \tan[\pi J_{CH_i} 2(T - \zeta)]\tan[\pi J_{CH_i} 2(T - \xi)] \\ &\approx \tan^2[\pi J_{CH_i}(2T - \zeta - \xi)] \end{aligned} \tag{3}$$

allowing a straightforward calculation of J_{CH_i}. The normalization factor has not been included in Eq. (3). Note that for valines and leucines, the intensity of the long-range correlation to the geminal methyl group needs to be divided by 3 prior to using Eq. (3) because it represents the superposition of three correlations to each of the three individual methyl protons.

Figure 11 shows examples of F_2 strips taken from the LRCH 3D spectrum of calmodulin, again complexed with the 26-residue peptide fragment. Figure 11A compares the two strips observed for the $C^{\gamma 2}$ and C^{δ} methyl resonances of Ile-52. Both methyl carbons show correlations to both $C^{\gamma 1}H_2$ methylene protons and to $C^{\beta}H$. The fact that $C^{\gamma 2}$ shows intermediate couplings of approximately 4 Hz to both $C^{\gamma 1}$ methylene protons, and that C^{δ} shows a 3.6 Hz coupling to H^{β} is indicative of motional averaging about the χ_2 angle. Indeed, the smaller-than-trans $C^{\delta}-C^{\alpha}$ J coupling (2.1 Hz) corroborates this conclusion.

Figure 11B shows long-range correlations to the C^{δ} methyl carbons of Leu-48. Stereospecific assignments of the H^{β} protons could be made on the basis of $H^{\beta}-^{15}N$ and $H^{\beta}-^{13}CO$ J couplings, using the above-described HNHB and HN(CO)HB experiments. Together with the observation that the $C^{\delta 1}$ methyl carbon shows a large coupling to $^{13}C^{\alpha}$, stereospecific assignments of the two methyl groups can be made. The fact that the $C^{\delta 2}-H^{\beta 2}$ J coupling (5.7 Hz) is somewhat smaller than what is expected for a

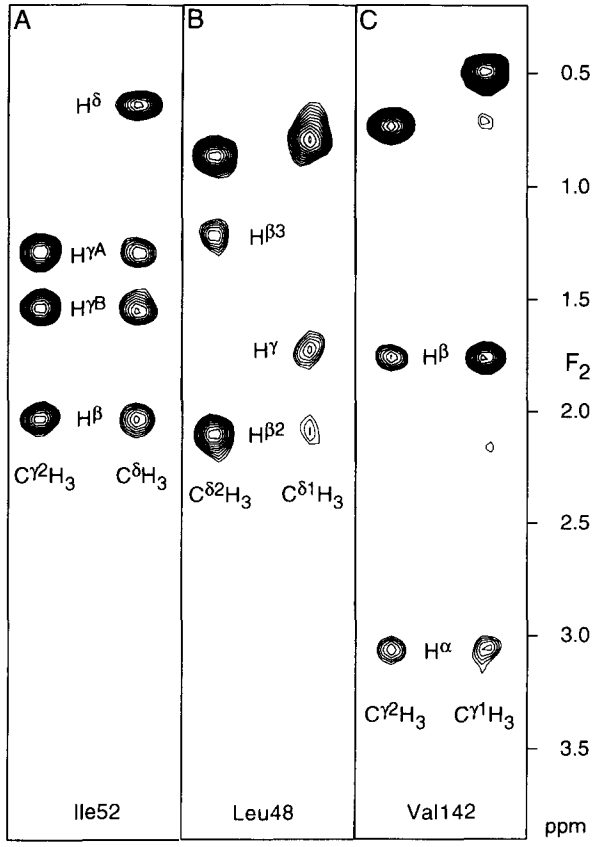

FIG. 11. Six F_2 strips from the 3D ^{1}H-detected [^{13}C–^{1}H] long-range correlation spectrum of calmodulin, complexed with a 26-residue peptide. The strips are taken at the (F_1, F_3) resonance frequencies of (A) $C^{\gamma 2}H_3$ and $C^{\delta 1}H_3$ of Ile-52, (B) $C^{\delta 2}H_3$ and $C^{\delta 1}H_3$ of Leu-69, and (C) $C^{\gamma 2}H_3$ and $C^{\gamma 1}H_3$ of Val-91. The strips show the resonances of all protons with a significant (>~2 Hz) coupling to the six methyl carbons. One-bond J correlations are suppressed, except for Ile-52 $C^{\delta}H_3$ and Val-142 $C^{\gamma 1}H_3$. (From Vuister and Bax.[31])

trans coupling, and the $C^{\delta 2}$–$H^{\beta 3}$ J coupling (3.5 Hz) is larger than what is expected for a gauche coupling, is probably caused by rapid spin flips between the strongly dipolar coupled H^{β} methylene protons. As previously discussed in some detail,[25] these spin flips have the effect of increasing the smaller of the two couplings and decreasing the larger one.

Figure 11C shows the connectivities observed for the Val-142 methyl carbons. Both methyl carbons show only very weak couplings (2.3 and 3.0 Hz) to H^{α}, as expected on the basis of the χ_1 angle of 180°, derived before from the large $^{13}C^{\gamma 1}$–^{15}N and $^{13}C^{\gamma 2}$–^{13}CO couplings.

Measurement of H^N–H^α J Couplings

To date, homonuclear three-bond $J_{H^NH^\alpha}$ couplings have been widely used in protein structural studies. They provide important information about the dihedral backbone angle ϕ. In small proteins they have been relatively easy to measure from the highly dispersed H^N–H^α fingerprint region of a phase-sensitive COSY spectrum.[32] Pardi *et al.*[33] have parameterized a Karplus function for this coupling by using values measured for basic pancreatic trypsin inhibitor (BPTI) and relating these to the ϕ angles of a high-resolution crystal structure. In larger proteins, accurate measurement of homonuclear J couplings is fraught with problems that are related to the small size of these couplings relative to the natural proton line width. In particular for proteins larger than about 10 kDa, quantitative measurement of homonuclear J couplings can be problematic.

A variety of methods have been proposed to address this problem. These include fitting procedures for the measurement of antiphase doublet splittings in COSY-type spectra,[2] ECOSY-type triple-resonance experiments on proteins uniformly enriched with both ^{13}C and ^{15}N,[17,18,34] measurement of the splitting in resolution-enhanced ^{15}N–^1H HMQC spectra,[3] nonlinear fitting of J-modulated ^{15}N–^1H HSQC spectra,[5] and fitting of in-phase splittings in 2D spectra.[35] Although some of these methods are more robust than others, all but the $^{15}N/^{13}C$-based ECOSY techniques decrease in accuracy when the line width becomes significantly larger than the J coupling. Especially for the measurement of small J couplings, such as typically encountered in α-helical regions of a protein ($J_{H^NH^\alpha} \sim 4$ Hz), this frequently presents a problem. The ECOSY-type experiments do not require the coupling to be resolved, but the precision with which J values can be measured is limited by the accuracy with which peak positions can be determined in 3D NMR spectra. In all these experiments, the value of the measured J coupling is also influenced by the rate of ^1H–^1H spin diffusion.[36] The method for measurement of the $J_{H^NH^\alpha}$ coupling described below relies on quantitative analysis of the diagonal to cross-peak intensity ratio in an ^{15}N-separated H^N–H^α homonuclear J correlation experiment.[37] In analogy with the nomenclature commonly used for related triple-

[32] D. Neuhaus, G. Wagner, M. Vasak, J. H. R. Kägi, and K. Wüthrich, *Eur. J. Biochem.* **151,** 257 (1985).

[33] A. Pardi, M. Billeter, and K. Wüthrich, *J. Mol. Biol.* **180,** 741 (1984).

[34] P. Schmieder, V. Thanabal, L. P. McIntosh, F. W. Dahlquist, and G. Wagner, *J. Am. Chem. Soc.* **113,** 6323 (1991).

[35] T. Szyperski, P. Güntert, G. Otting, and K. Wüthrich, *J. Magn. Reson.* **99,** 552 (1992).

[36] G. Harbison, *J. Am. Chem. Soc.* **115,** 3026 (1993).

[37] G. W. Vuister and A. Bax, *J. Am. Chem. Soc.* **115,** 7772 (1993).

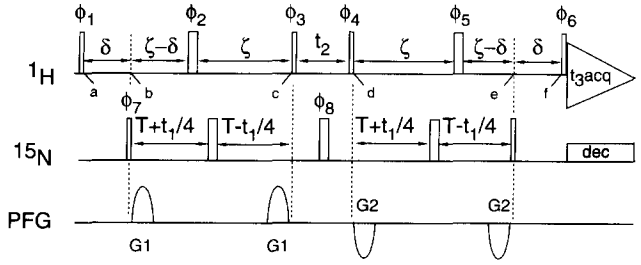

FIG. 12. Pulse scheme of the 3D HNHA experiment. Narrow and wide pulses denote 90° and 180° flip angles, respectively. Unless indicated otherwise, all pulses are applied along the x axis. The following phase cycle is used: $\phi_1 = x$; $\phi_2 = 4x,4(-x)$; $\phi_3 = x,-x$; $\phi_4 = 2x,2(-x)$; $\phi_5 = 4x,4(-x)$; $\phi_6 = y,-y$; $\phi_7 = x$; $\phi_8 = 8x,8y$; receiver: $8x,8(-x)$. Quadrature detection in t_1 and t_2 is obtained with the States–TPPI method, incrementing phases ϕ_7 for t_1 and phases ϕ_1, ϕ_2, and ϕ_3 for t_2. Pulsed-field gradients (PFGs) have a sine bell shape with a strength of 10 G/cm at the maximum and are applied along the z axis. PFG durations are $G_1 = 750$ μsec and $G_2 = 750$ μsec (negative polarity). The delay δ is set to 4.5 msec, and the delay ζ is set to 13.05 msec. Solvent suppression is achieved by irradiation with a weak rf-field ($\gamma B_2 \sim 25$ Hz) during the relaxation delay. (From Vuister and Bax.[37])

resonance experiments, the experiment is named HNHA as it correlates the intraresidue $^1H^N$, ^{15}N, and $^1H^\alpha$ resonances.

The HNHA pulse scheme is shown in Fig. 12 and is briefly discussed below. A more complete description of the pulse sequence, using the product operator formalism, is presented elsewhere.[37] For the present discussion it suffices to consider a simple system comprised of the proton amide spin (H^N), the H^α proton spin coupled to H^N with coupling constant J_{HH}, and the ^{15}N spin coupled to H^N with a coupling constant $_{NH}$. Proton magnetization, generated by the first $90°_{\phi_1}$ ^1H pulse and present at time a in Fig. 12, dephases with respect to its attached ^{15}N spin during the delay δ. Zero- and double-quantum terms are generated by the $90°_{\phi_7}$ (^{15}N) pulse applied at time b in a heteronuclear multiple-quantum correlation spectroscopy (HMQC) type fashion.[38,39] Simultaneous displacement of the first and third 180° ^{15}N pulses during the subsequent delays, of total duration $4T + t_2$, causes labeling with the chemical shift of the ^{15}N spin in a "constant-time" manner.[40,41] No labeling by $^1J_{NH}$ takes place because evolution of the zero- and double-quantum terms is not affected by the one-bond J coupling between the H^N and ^{15}N spins.

[38] L. Mueller, *J. Am. Chem. Soc.* **101,** 4481 (1979).
[39] A. Bax, R. H. Griffey, and B. L. Hawkins, *J. Magn. Reson.* **55,** 301 (1983).
[40] O. W. Sørensen, *J. Magn. Reson.* **90,** 433 (1990).
[41] R. Powers, A. M. Gronenborn, G. M. Clore, and A. Bax, *J. Magn. Reson.* **94,** 209 (1991).

Between time points a and c, dephasing occurs as result of the homonuclear H^N–H^α J coupling active for a total duration 2ζ. As a result, terms develop that contain amide proton magnetization which is antiphase with respect to the H^α spin and which are proportional to $\sin(2\pi J_{HH}\zeta)$. The amide antiphase term subsequently is converted to antiphase H^α magnetization by the $90°_{\phi_3}$ ^1H pulse. After the short t_2 evolution period, antiphase H^α magnetization terms are converted back to antiphase amide magnetization. During the subsequent rephasing period between time points d and f, homonuclear H^N–H^α J coupling is active again, and rephasing proportional to $\sin(2\pi J_{HH}\zeta)$ occurs. The $90°(^{15}N)$ pulse applied at time e converts multiple-quantum terms back to amide magnetization antiphase with respect to its attached ^{15}N spin. The antiphase magnetization subsequently rephases during the final δ delay. Because a $90°_{\phi_6}$ purge pulse is applied immediately prior to data acquisition, only amide proton magnetization that originates from in-phase terms is observed during t_3, and the signal $S(t_1, t_2, t_3)$ is described by

$$S(t_1, t_2, t_3) = A[\cos^2(2\pi J_{HH}\zeta)\cos(\omega_N t_1)\cos(\omega_{HN} t_2) - \sin^2(2\pi J_{HH}\zeta)\cos(\omega_N t_1)\cos(\omega_\alpha t_2)] \exp(i\omega_{HN} t_3) \quad (4)$$

where ω_{HN}, ω_N, and ω_α are the angular offset frequencies of the amide proton, amide nitrogen, and H^α proton, respectively. The constant A includes a product of trigonometric functions of the one-bond heteronuclear nitrogen–proton coupling and the heteronuclear two-bond and three-bond ^{15}N–H^α couplings active during parts of the pulse sequence.[37]

In the F_1 and F_3 dimensions, the line shapes of the "diagonal peak" at $(F_1, F_2, F_3) = (\omega_N, \omega_{HN}, \omega_{HN})$ and the cross-peak at $(F_1, F_2, F_3) = (\omega_N, \omega_\alpha, \omega_{HN})$ are determined by identical factors. In the F_2 dimension, the intrinsic line widths of the diagonal peak and cross-peak are determined by the decay rates of transverse H^N and H^α magnetization during t_2. However, since the acquisition time in the t_2 dimension is much shorter than the transverse relaxation time of either H^N or H^α, the line shape in the F_2 dimension is determined primarily by the apodization function used in the t_2 dimension. Therefore, diagonal peaks and cross-peaks also have nearly identical line shapes in the F_2 dimension, and the intensity ratio S_{cross}/S_{diag} provides a direct measure for J_{HH}:

$$S_{cross}/S_{diag} = -\tan^2(2\pi J_{HH}\zeta) \quad (5)$$

The HNHA experiment offers excellent sensitivity, in spite of the long dephasing and rephasing delays 2ζ. As an example of the spectral quality,

Fig. 13 shows seven F_2 strips from the HNHA spectrum of uniformly ^{15}N-labeled staphylococcal nuclease (SNase), taken at the ^{15}N–^{1}H resonance frequencies of residues Tyr^{85}–Tyr^{91}. The F_2 region between 7.0 and 9.5 ppm contains the "diagonal" peaks corresponding to magnetization not transferred to H$^\alpha$ during t_2. The cross-peaks between amides and H$^\alpha$ resonances are located in the F_2 region between 3.5 and 5.5 ppm. Owing to the 3D nature of the experiment and the high resolution obtainable in the constant-time ^{15}N dimension, cross-peaks are virtually free of overlap. Overlap of the "diagonal" resonances is comparable to that in a high-resolution 2D ^{1}H–^{15}N correlation spectrum.

In deriving Eq. (5), the implicit assumption is made that during the

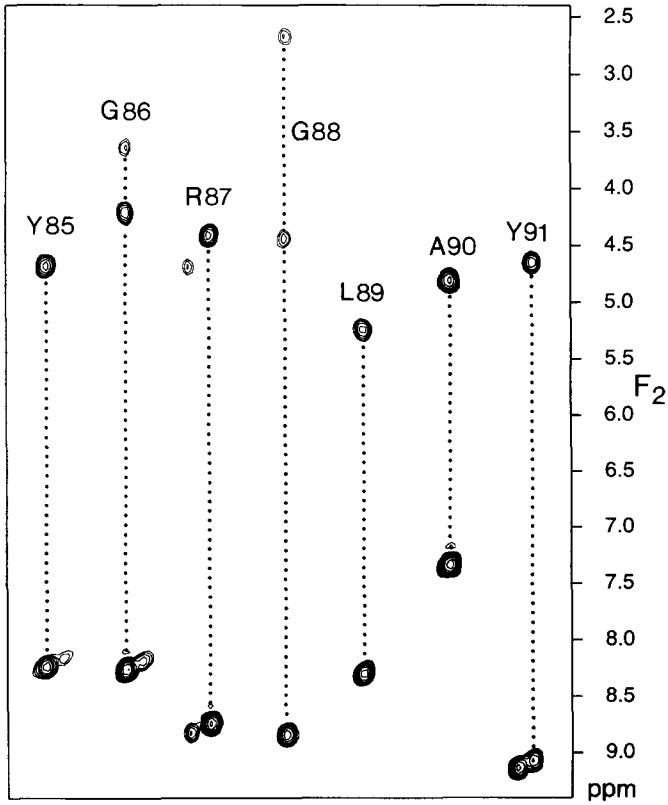

FIG. 13. Several F_2 strips from the 3D HNHA spectrum of uniformly ^{15}N-enriched staphylococcal nuclease, taken at the ^{15}N–^{1}H resonance positions of Tyr^{85}–Tyr^{91}. Resonances in the F_2 region between 3.5 and 5.5 ppm are H^N–H$^\alpha$ cross-peaks with negative intensities, and resonances downfield of F_2 = 7 ppm are H^N diagonal peaks with positive intensities. The cross-peak to diagonal-peak intensity ratio presents a measure for the ^3J(H^{N}H$^\alpha$) coupling. (From Vuister and Bax.[37])

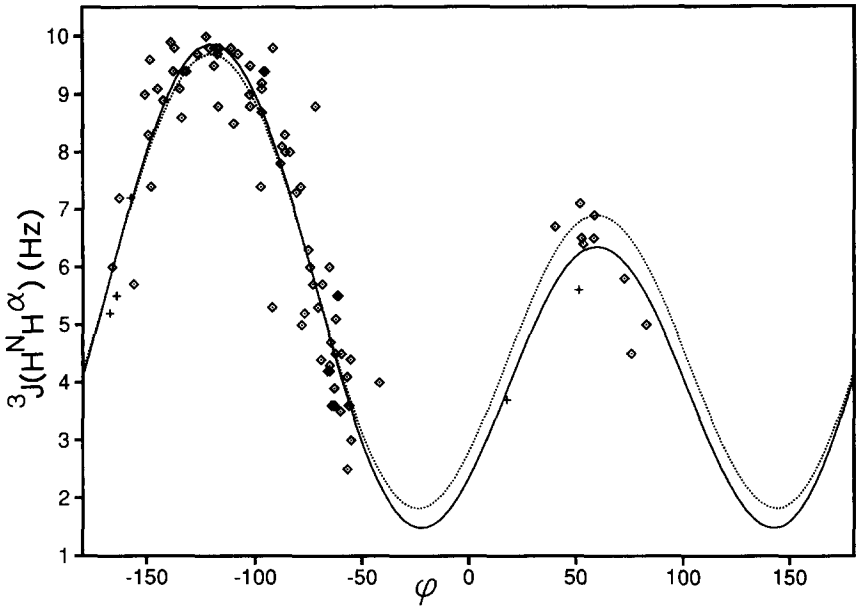

FIG. 14. Measured values for 94 $^3J(H^NH^\alpha)$ coupling constants obtained from the HNHA spectrum of staphylococcal nuclease, plotted as a function of the backbone angle ϕ. $^3J(H^NH^\alpha)$ couplings to the $H^{\alpha 3}$ of glycine residues are marked +. The backbone angle ϕ is offset by 120° for these data points. The solid line indicates the least-squares minimized fit of the Karplus curve $J = A\cos^2(\phi - 60°) + B\cos(\phi - 60°) + C$, with $A = 6.51$, $B = -1.76$, and $C = 1.60$ and a rms deviation of 0.73 Hz.[37] The dotted line corresponds to the Pardi parameterization,[33] with $A = 6.4$, $B = 1.4$, and $C = 1.9$, and a rms deviation of 0.76 Hz.

de- and rephasing delays, 2ζ, the magnetization components giving rise to diagonal peaks and cross-peaks relax at identical rates. If the amide spin is described by an operator $\mathbf{I}^N$ and the H^α spin by $\mathbf{I}^\alpha$, it is well known that antiphase magnetization of the form $2\mathbf{I}^N{}_x\mathbf{I}^\alpha{}_z$ relaxes faster than the in-phase component $\mathbf{I}^N{}_y$.[42-44] For proteins in the slow motion limit, the relaxation time of the antiphase magnetization (T_{2ap}) to a good approximation is given by

$$T_{2ap} = (T_{2HN}{}^{-1} + T_{1sel}{}^{-1})^{-1} \tag{6}$$

where T_{2HN} is the transverse relaxation time of the in-phase H^N magnetization and T_{1sel} is the selective T_1 of the H^α spin, which is primarily determined by cross-relaxation with other protons. The value of T_{1sel} can be

[42] A. Bax, M. Ikura, L. E. Kay, D. A. Torchia, and R. Tschudin, *J. Magn. Reson.* **86,** 304 (1990).
[43] R. E. London, *J. Magn. Reson.* **86,** 410 (1990).
[44] J. Peng, V. Thanabal, and G. Wagner, *J. Magn. Reson.* **95,** 421 (1991).

TABLE I
DIHEDRAL ANGLES IN PROTEINS THAT CAN BE STUDIED BY QUANTITATIVE *J* CORRELATION EXPERIMENTS

Experiment	Angle	Residues	Refs.
HNHB	χ_1, ψ	All[a]	23, 46
HN(CO)HB	χ_1, ϕ	All[b]	24
LRCC	χ_1	Thr, Ile, Val[c]	27
	χ_2	Leu[c]	
LRCH	χ_1	Thr, Ile, Val[c]	25, 31
	χ_2	Leu[c]	
^{13}C–{^{15}N}–SED[d]	χ_1	Thr, Ile, Val[c]	28
^{13}C–{^{13}CO}–SED[d]	χ_1	Thr, Ile, Val[c]	47
HNHA	ϕ	All[a]	37

[a] All residues except prolines and residues with rapidly exchanging amide protons.
[b] All residues except those followed by prolines or residues with rapidly exchanging amide protons.
[c] Also applicable to other residues in small proteins.
[d] SED–Spin echo difference.

derived indirectly from the difference in relaxation between I_z terms and I_zS_z terms. Using this approach, T_{1sel} values of around 125 msec are found for the H^N protons in SNase.[45] Values in the range 100–200 msec are found for the H^α protons of alanine residues in nonflexible parts of [$^{13}C^\alpha$–Ala]SNase (L. K. Nicholson and D. A. Torchia, unpublished results).

Because the H^N–H^α cross-peaks and the H^N–H^N diagonal peaks result from the antiphase and in-phase terms, respectively, the faster relaxation of the antiphase $2\mathbf{I}^N{}_x\mathbf{I}^\alpha{}_z$ term attenuates the cross-peak relative to the diagonal peak, resulting in an underestimate of the *J* coupling. However, as shown elsewhere,[37] the fractional error in the derived *J* coupling caused by this relaxation effect is, to a good approximation, independent of the size of the coupling, and it can be corrected for in a straightforward way if an estimate for the H^α flip rate is available. For SNase, with a rotational correlation time of 9 nsec, a uniform increase by 11% of the *J* couplings obtained using Eq. (5) shows excellent agreement with values predicted from the Karplus relation parameterized by Pardi *et al.*,[33] yielding a root mean square (rms) deviation of only 0.76 Hz (Fig. 14).

The quantitative *J* correlation HNHA experiment allows the precise

[45] L. E. Kay, L. K. Nicholson, F. Delaglio, A. Bax, and D. A. Torchia, *J. Magn. Reson.* **97,** 359 (1992).
[46] J. C. Madsen, O. W. Sørensen, P. Sørensen, and F. M. Poulsen, *J. Biomol. NMR* **3,** 239 (1993).
[47] S. Grzesiek, G. W. Vuister, and A. Bax, *J. Biomol. NMR.* **3,** 487 (1993).

measurement of very small J values, even in proteins of substantial size. The experiment therefore also provides a sensitive way for J-correlating the intraresidue H^N and H^α resonances, a prerequisite for establishing protein sequential assignment.

Conclusions

Quantitative J correlation is a useful and general approach for measuring a large variety of two- and three-bond homo- and heteronuclear J couplings, providing access to the study of a large number of dihedral angles in proteins (Table I). The approach is not limited to isotopically enriched proteins and has also been used to measure a large number of heteronuclear ^1H–^{13}C J couplings in the cyclic decapeptide gramicidin S.[48]

The quantitative J correlation experiments are particularly useful for defining the χ_1 angle, as a substantial number of J couplings defined by this angle can now be measured. For valine residues, for example, six J couplings are readily available and, in addition the H^α–H^β J coupling may in favorable cases be measurable by other techniques. This large number of J couplings overdetermines χ_1 if there exists only a single rotameric state. In cases of rotamer averaging, however, this large number of independent J measurements provides a unique opportunity to characterize the motional averaging process.

The complexity of the J correlation spectra is low compared to alternative ECOSY type experiments as no additional passive coupling is needed. However, as the J coupling is measured from the intensity of its corresponding long-range correlation, there exists a lower limit below which quantitative J correlation cannot provide the J value. The same limitation does not apply to ECOSY-based schemes, where couplings of 0.1 Hz are measured with the same ease as 5 or 10 Hz couplings. For the proteins we have studied, in the range 15–20 kDa, the lower limit measurable for ^{15}N–$^1H^\beta$, ^{13}CO–$^1H^\beta$, and $^{13}C(H_3)$–^1H three-bond couplings is about 1.5–2 Hz. For the $^{13}C(H_3)$–^{15}N and $^{13}C(H_3)$–^{13}C J couplings, the lower limits are about 0.5 and 1 Hz, respectively. The lower limit measurable for H^N–H^α J values is about 3 Hz. For proteins with rotational correlation times shorter than those used in the present work, or for proteins significantly more concentrated than 1–1.5 mM, the above-mentioned lower limits of measurable couplings may be considerably smaller.

Acknowledgments

We thank Marius Clore, Angela Gronenborn, and Dennis Torchia for numerous stimulating discussions. This work was supported by the AIDS Targeted Anti-Viral Program of the Office of the Director of the National Institutes of Health.

[48] G. Zhu and A. Bax, *J. Magn. Reson. Ser. A* **104,** 353 (1993).